agronomy

MDPI

Article

Analysis of Vegetation Dynamics and Phenotypic Differentiation in Five Triticale (×*Triticosecale Wittm.*) Varieties Using UAV-Based Multispectral Indices

Asparuh I. Atanasov [1], Hristo P. Stoyanov [2], Atanas Z. Atanasov [3,*] and Boris I. Evstatiev [4]

[1] Department of Mechanics and Elements of Machines, Technical University of Varna, 9010 Varna, Bulgaria; asparuh.atanasov@tu-varna.bg
[2] Dobrudzha Agriculture Institute—General Toshevo, Agricultural Academy, 9521 General Toshevo, Bulgaria; hpstoyanov@abv.bg
[3] Department of Agricultural Machinery, Agrarian and Industrial Faculty, University of Ruse "Angel Kanchev", 7017 Ruse, Bulgaria
[4] Department of Automatics and Electronics, Faculty of Electrical Engineering, Electronics, and Automation, University of Ruse "Angel Kanchev", 7017 Ruse, Bulgaria; bevstatiev@uni-ruse.bg
* Correspondence: aatanasov@uni-ruse.bg

Abstract

This study investigates the vegetation dynamics and phenotypic differentiation of five triticale (×*Triticosecale Wittm.*) varieties under the region-specific agroecological conditions of Southern Dobruja, Bulgaria, across two growing seasons (2024–2025), with the aim of evaluating how local climatic variability shapes vegetation index patterns. UAV-based multispectral imaging was employed throughout key phenological stages to obtain reflectance indices, including NDVI, SAVI, EVI2, and NIRI, which served as indicators of canopy development and physiological status. NDVI was used as the primary reference index, and a baseline value (NDVIbase), defined as the mean NDVI across all varieties on a given date, was applied to evaluate relative varietal deviations over time. Multiple linear regression analyses were performed to assess the relationship between NDVI and baseline biometric parameters for each variety, revealing that varieties 22/78 and 20/52 exhibited reflectance dynamics most closely aligned with expected developmental trends in 2025. In addition, the relationship between NDVI and meteorological variables was examined for the variety *Kolorit*, demonstrating that relative humidity exerted a pronounced influence on index variability. The findings highlight the sensitivity of triticale vegetation indices to both varietal characteristics and short-term climatic fluctuations. Overall, the study provides a methodological framework for integrating UAV-based multispectral data with meteorological information, emphasizing the importance of region-specific, time-resolved monitoring for improving precision agriculture practices, optimizing crop management, and supporting informed variety selection.

Keywords: precision agriculture; remote sensing; vegetation indices; analysis; NDVI; SAVI; EVI2; NIRI

Check for updates

Received: 21 December 2025
Revised: 12 January 2026
Accepted: 22 January 2026
Published: 25 January 2026

Copyright: © 2026 by the authors. Licensee MDPI, Basel, Switzerland. This article is an open access article distributed under the terms and conditions of the Creative Commons Attribution (CC BY) license.

1. Introduction

Triticale (×*Triticosecale Wittm.*) is a highly productive cereal that combines the baking qualities of wheat with the ecological adaptability and disease and pest-resistance traits of rye. The growing global population and the consequent increase in food demand have intensified the interest in this crop. The adoption of advanced cultivation technologies and

intelligent monitoring systems has contributed to an increase in triticale yields, which now exceed 14 million tons worldwide [1]. In the context of climate variability, cereal breeders face the challenge of developing cultivars with enhanced vigor, drought tolerance, and resistance to economically significant diseases and pests. Recent innovations in precision agriculture—including the use of the Internet of Things (IoT), unmanned aerial vehicles (UAVs), satellite-based monitoring, and deep learning algorithms—are exerting a pivotal influence on triticale production and breeding strategies.

Reflectance-based vegetation indices provide essential information about the physiological condition and developmental stage of crops. Their potential application for varietal differentiation is of particular importance in precision agriculture. Advances in technology, together with improvements in multispectral imaging and deep learning algorithms, have provided powerful tools for distinguishing crop varieties and predicting developmental parameters [2]. By leveraging predictive data generated through machine learning, farmers can make timely and informed decisions regarding forthcoming agrotechnical interventions [3]. The detection and classification of crop species and varieties, as well as the extraction of relevant phenotypic traits from UAV-acquired imagery, can be achieved through optimized machine learning workflows, thereby enabling the creation of integrated systems for assessing overall plant health [4]. Recent UAV-based cereal phenotyping studies have demonstrated the utility of multispectral imagery for characterizing growth dynamics and estimating heritable traits in wheat and other cereals [5]. Moreover, real-time monitoring can be facilitated through IoT-based systems. For example, a fertilizer recommendation module developed in Python 3.14.2 (Flask, HTML, CSS, JavaScript, Bootstrap) compares user-input soil data with optimal nutrient parameters to support precision fertilization decisions [6].

Multi-temporal Sentinel-2 imagery was used in [7] to conduct a vegetation cover classification based on visual and numerical comparisons between the studied agricultural areas and ground reference data. The method demonstrated high reliability in generating polygons that closely corresponded to the reference datasets. The results showed that the normalized difference vegetation index (NDVI) provides valuable information on the predominant vegetation cover and enables the modeling of phenological stages across various crops. NDVI calculations for the regions of interest (ROIs) clearly delineate vegetation types within the study area.

Advances in multispectral imaging technology and the improvement of spatial resolution have facilitated the acquisition of increasingly accurate raw data. The accuracy of reflectance and vegetation indices (VIs) obtained from UAV-mounted sensors can be used for the simultaneous evaluation and collection of multispectral imagery; furthermore, when combined with soil, crop, and climatic data, the NDVI allows for detailed, plot-level analyses. Therefore, multispectral remote sensing is becoming an established standard in modern crop monitoring and analysis [8]. Similar UAV-based studies have successfully applied multispectral imaging to barley and other cereals, enabling high-throughput phenotypic assessments and supporting breeding programs [9]. Different studies have discussed the capabilities of robotic UAVs for the monitoring of crops of carrying sizes and the influence of their image sensors [10,11]. Previous studies have shown that the collected datasets can be used to assess crop stress [12], detect weed infestations [13], identify soil type [14], evaluate moisture availability [15], and monitor pathogen presence [16], along with other factors influencing overall crop performance.

Given that the factors influencing crop growth—such as soil properties, climatic conditions, and agroecological interactions—are highly region-specific and may vary substantially from year to year, there is a clear need for the systematic, long-term monitoring of triticale varieties under local environmental conditions.

In the specific agro-climatic conditions of the historical-geographical region of Southern Dobruja, the dynamics of triticale development, assessed via vegetation indices, have not been studied to date. The region is predominantly cultivated with maize, sunflower, and winter wheat, while triticale cultivation is still emerging. Sowing occurs in spring, but the area is prone to typical spring frosts, which may affect crop development. Conversely, summer temperatures can reach 40 °C and are often accompanied by prolonged droughts. These features create distinct regional conditions that influence the physiological development of crops.

The advent of accessible multispectral cameras allows for the independent monitoring of experimental plots, which is particularly useful for breeding programs with small research fields that cannot be effectively assessed via satellite imagery. These cameras can be used independently or mounted on small UAVs, enabling flexible, high-resolution, and non-invasive phenotyping.

The primary objective of this study is to quantify the vegetation dynamics and phenotypic differentiation of five triticale (×*Triticosecale Wittm.*) varieties under the specific agroecological conditions of the growing region by integrating UAV-based multispectral indices with meteorological parameters over two consecutive growing seasons. To achieve this goal, the following specific tasks were undertaken:

1. Planning and establishing the field experiment, including sowing and experimental design.
2. Conducting multispectral analyses using UAV imagery to examine trends in four key vegetation indices (NDVI, SAVI, EVI2, and NIRI).
3. Monitoring and recording meteorological parameters alongside soil sample data.
4. Analyzing the relationships between the collected variables to assess varietal responses and environmental influences.

2. Materials and Methods

2.1. Study Area

The study was conducted at the experimental field of the Dobruja Technological College, city of Dobrich, Republic of Bulgaria, with coordinates 43.553343°, 27.832156°, as shown in Figure 1.

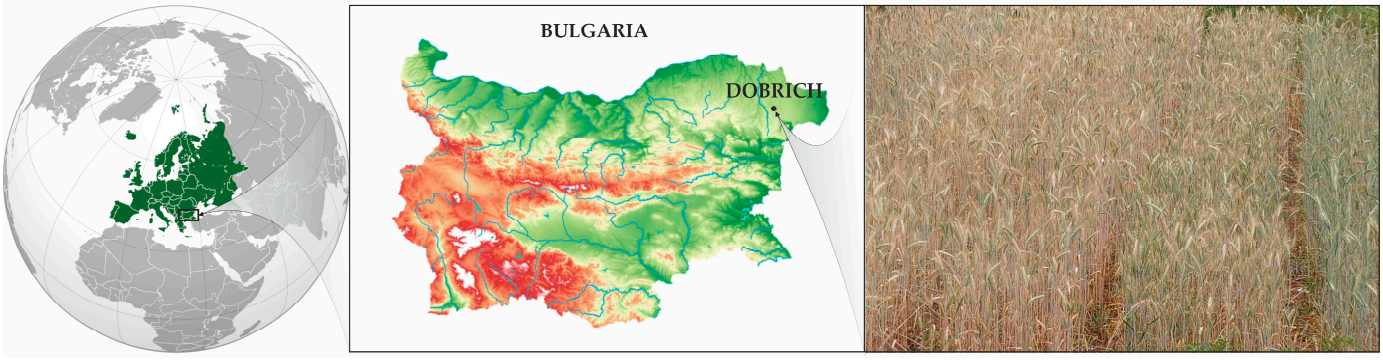


Figure 1. Experiment location (Adobe Photoshop version 26.0.0 was used).

The study's object comprises five triticale (×*Triticosecale Wittm.*) varieties. The experimental field is designated for testing both newly selected and existing varietal selections under real field conditions. The observation period encompassed the entire vegetation cycle of triticale during the 2024 and 2025 growing seasons.

The sowing layout of the 2024 experiment is presented in Figure 2. The columns, labeled with Roman numerals, correspond to the tested varieties: I—variety *17/5*; II—variety *20/52*; III—variety *22/78*; IV—variety *22/71*; and V—variety *Kolorit*. The rows, numbered with Arabic numerals, indicate the replication number. In the 2025 season, the experimental design maintained the same configuration, with three replications instead of five.

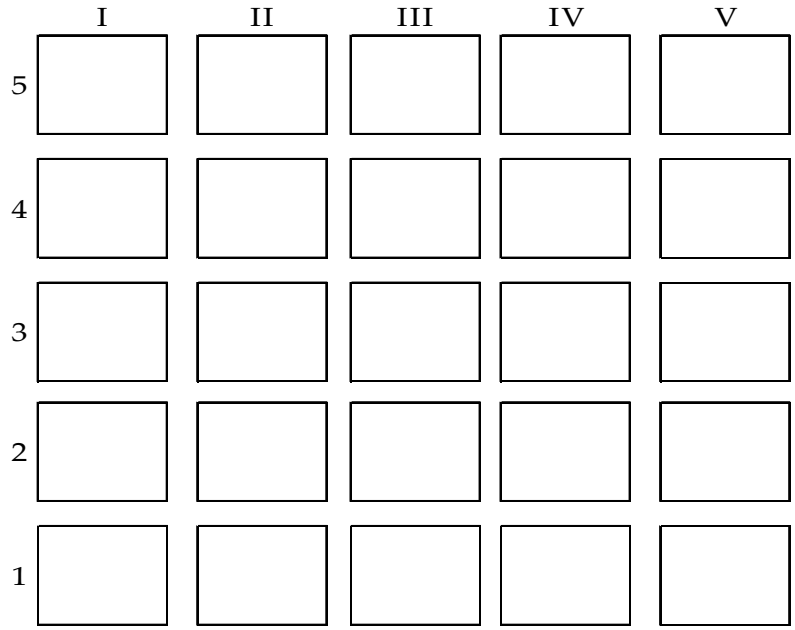


Figure 2. Seeding plan for the experiment.

The *Kolorit* variety was included as a reference standard due to its established adaptation to the local agro-climatic conditions, providing a benchmark for evaluating the performance and spectral dynamics of the newly selected lines.

2.2. Research Methodology

Soil composition was analyzed using a USB portable soil parameter detector, (NiuBoL, Guangzhou, China). which measures moisture, soil temperature, electrical conductivity, pH, fertility, nitrogen, phosphorus, and potassium. The device operates within the following ranges: moisture, 0–100%; electrical conductivity, 0–20,000 µS/cm; NPK, 0–2000 mg/kg; and pH, 0–14. Measurements were conducted in the topsoil up to a depth of 150 mm.

Light properties were measured using an HPCS-320 spectrometer (Zhejiang Hopoo Light & Color Technology Co., Ltd., Xihu District, Hangzhou, Zhejiang Province, China) [17]. The HPCS-320 series optical spectrum analyzer features a high-precision CCD optical sensor and a 3.5-inch touchscreen display. Sampling and measurement of the light source can be performed in real time and in the field, with high-efficiency analysis and processing. Various solar radiation parameters were recorded.

Wind speed, air temperature, and relative humidity were measured using an anemometer–thermometer–hygrometer VA8021 [18]. The device specifications are as follows: wind speed, 0.4–20 m/s; temperature, −10 to 50 °C; and relative humidity, 0–100% RH. The instrument allows for the selection of different units (wind speed: m/s, km/h, fpm, mph, and kts; temperature: °C, °F; and humidity: %RH, dew point temperature) and is equipped with an LCD, automatic shutdown, Data Hold, MIN/MAX functions, backlight, out-of-range indication, and low-battery alert.

During field surveys, meteorological conditions were recorded prior to measurements to ensure the observations were properly conducted. The recorded parameters included air temperature (°C), illumination (kLx), wind speed (m/s), relative humidity (%RH), color temperature (CCT, K), and peak solar radiation wavelength (nm).

Plant measurements were performed for each variety. Stem height was measured in the field and validated by individual plot observations. To determine grain and spike characteristics at maturity, spike samples were collected by variety, processed, and analyzed to extract the necessary morphological and yield parameters.

2.3. Method for Obtaining Reflective Vegetation Indices

The study utilized the *NDVI* [19] as one of the most widely applied vegetation reflectance indices. It is commonly used to assess vegetation density, monitor crop health, detect stress, evaluate weed presence, and predict yields, and is calculated based on the ratio between the red and near-infrared spectral bands. Specifically, the reflectance at 0.66 μm, corresponding to maximum chlorophyll absorption, and the reflectance at 0.85 μm in the near-infrared region are used in the following calculation:

$$NDVI = \frac{R_n - R_r}{R_n + R_r} \quad (1)$$

where R_n represents reflectance in the near-infrared spectral band and R_r represents reflectance in the red spectral band.

NDVI serves as an indicator of plant condition and stress presence, although it does not provide information on the specific causes of observed variation. Early in the season, the *NDVI* can be used to assess how plants have overwintered. However, the *NDVI* may be influenced by soil background, particularly in areas with sparse vegetation. To account for this effect, the Soil-Adjusted Vegetation Index (*SAVI*) [20] was also calculated, which corrects for soil brightness and provides a more accurate assessment of vegetation condition under low canopy cover:

$$SAVI = \frac{(1 - L)(R_n - R_r)}{R_{n+}R_r + 0.5} \quad (2)$$

where L is a soil brightness correction factor. In this study, a value of L = 0.5 was adopted, corresponding to intermediate vegetation density.

The factor L serves to reduce soil background influence for all types of vegetation, while the multiplication factor $(1 - L)$ dynamically adjusts the index. As demonstrated in [19], the value of L decreases with increasing vegetation density:

- L = 1 for very sparse vegetation;
- L = 0.5 for intermediate vegetation density;
- L = 0.25 for dense vegetation cover.

SAVI is particularly recommended for analyzing crops in the initial stages of vegetation development, in dry regions with sparse vegetation (<15% coverage), or in areas with exposed soil surfaces.

The Enhanced Vegetation Index 2 (*EVI2*) [21,22] is designed to minimize the influence of atmospheric effects on remote-sensing data and improve sensitivity in areas with high biomass by reducing background noise. It is particularly useful for detecting differences in growth dynamics and monitoring crop development under high-density vegetation conditions:

$$EVI2 = 2.5 \frac{R_n - R_r}{R_n + 2.4R_r + 1} \quad (3)$$

The Near-Infrared Reflectance Index (*NIRI*) [23] is used during active wheat vegetation, when the reflectance in the near-infrared region significantly exceeds that in the visible spectrum. The *NIRI* allows for the assessment of vegetation by comparing near-infrared reflectance to the combined reflectance in the red and green bands, thereby reducing the influence of the soil background. The index is calculated as follows:

$$NIRI = \frac{R_n}{R_r + R_g} \quad (4)$$

where R_g is the green reflected light.

The expected value of the *NDVI* index for a given time period, reflecting climatic characteristics and the development dynamics of the *NDVI*base varieties, is determined using the following time series:

$$NDVI(t), (t = 1, 2, 3, \ldots, n) \quad (5)$$

where NDVI(t) denotes the actual NDVI value in year t. For each measurement obtained during the growing season, where $\tau = 1, 2, 3, \ldots, t$,

$$NDVI_{(\tau)} = \frac{1}{\tau} \sum_{t=1}^{\tau} NDVI_{(t)}\ t = 1,\ 2,\ 3,\ \ldots,\ n \quad (6)$$

t denotes the year of measurement; τ denotes measuring the index on a specific date in the year.

To assess temporal changes in the *NDVI* based on historical data, the *NDVI* base index was defined as the mean *NDVI* value across all observed varieties on a given date throughout the growing season. This approach eliminates varietal-specific physiological differences while capturing the overall trend of *NDVI* dynamics. For example, the *NDVI* value for 15 April 2025 is compared with the corresponding values for varieties 17/5, 20/52, 22/78, 22/71, and *Kolorit*. This allows for the calculation of relative deviations from the expected baseline, representing the typical growth dynamics for that date, independent of individual varietal variation. In this context, the *NDVI*base serves as a standard expected value, providing a benchmark for evaluating the performance and temporal development of individual varieties.

2.4. Method of Recording and Processing

Triticale was imaged using a multispectral camera from Mapir, (San Diego, CA 92126, United States) [24]. The Survey3W Camera—RGN was employed, capturing images in the near-infrared (850 nm), red (660 nm), and green (550 nm) spectral bands. The camera is equipped with a Sony (Headquarters - Minato, Tokyo, Japan) Exmor R IMX117 12MP (Bayer RGB) sensor and an 87° HFOV (19 mm) lens with f/2.8 aperture and −1% extreme low distortion (non-fisheye) glass. The resulting images have a resolution of 12 megapixels (4000 × 3000 px).

An external GPS/GNSS module (u-blox UBX-G7020-KT) was mounted on the camera to record georeferenced coordinates for each image. The camera setup is shown in Figure 3a, and an example of a captured image of an experimental plot in the RGN spectrum is presented in Figure 3b.

The DJI Phantom 4 Adv drone [25] was used solely as a platform for the Mapir multispectral camera; data from the drone's onboard camera were not analyzed. The flight altitude over the experimental plots was 12 m, selected due to the small size of the experimental field. The flight height and camera position were carefully adjusted

according to the plot dimensions, proportions, and the sensor resolution to ensure optimal image quality.



(**a**) (**b**)

Figure 3. Survey3W camera [22] (**a**) and an example of an image captured in the RGN spectrum (**b**).

For color calibration under variable solar illumination, a Diffuse Reflectance Standard Calibration Target Package (V2) from Mapir [24] was used. This calibration procedure ensures accurate spectral measurements and contributes to the reproducibility and reliability of the collected data, addressing critical experimental details for the study.

At the flight altitude of 12 m, the resulting ground sampling distance (GSD) of the images was approximately 1.5 cm per pixel, providing sufficient spatial resolution to capture plot-level vegetation dynamics.

The acquired images were processed using Pix4Dfields software (Pix4D S.A., Prilly, Switzerland, Version 2.8.5) [26] Computer vision laboratory of the Swiss Federal Institute of Technology Lausanne (EPFL) in Switzerland, which allows for georeferencing, mosaicking, and analysis of multispectral imagery for precision agriculture applications.

Image acquisition was planned to occur between 12:00 and 14:00 h to minimize the influence of cast shadows. During this interval, the color temperature is relatively uniform due to the maximum sunlight intensity. Flights were avoided on days with rain or snow, as precipitation could compromise data accuracy. Images were captured at a 1 s interval, while the UAV traveled at a speed of 5 km/h, ensuring an approximate 80% overlap between consecutive photos.

The raw images were imported into Pix4Dfields software for processing, which was conducted with an active internet connection. The maximum orthomosaic size was set, and the desired vegetation indices were specified within the program. This procedure generated a generalized map of the entire experimental field. To extract indices for individual varieties or plots, the respective areas were selected and reprocessed. The method was repeated separately for each variety, and the resulting indices were recorded.

Image acquisition was conducted weekly from the emergence of the triticale trial in April until mid-July, corresponding to crop maturity.

2.5. Triticale Varieties Studied

The study focused on the following triticale varieties:

- Four Mexican spring-type hexaploid triticale varieties from the CYMMIT collection: *17/5*, *20/52*, *22/78*, and *22/71*.

- *Kolorit*—a Bulgarian winter hexaploid triticale variety that can also be cultivated under spring conditions. *Kolorit* is characterized by high yield stability under favorable environmental conditions, rapid spring development, and relatively early emergence. The variety produces large, well-filled spikes with comparatively large grains.

2.6. Statistical Processing

The statistical analysis of the results was performed using multivariate linear regression in IBM SPSS Statistics 26 [27] (International Business Machines Corporation, Armonk, NY, USA). The dependent variable, the *NDVI* base (Y), was analyzed with respect to the following independent variables: X_1—*NDVI* variety *17/5*, X_2—*NDVI* variety *20/52*, X_3—*NDVI* variety *22/78*, X_4—*NDVI* variety *22/71*, and X_5—*NDVI* variety *Kolorit*. The corresponding regression equation is given as follows:

$$Y = a\,X1 + b\,X2 + c\,X3 + d\,X4 + e\,X5 + f \quad (7)$$

The dependent variable, the *NDVI* variety color (Y), was analyzed in relation to the following independent variables: X_1—soil moisture (%), X_2—air temperature (°C), and X_3—relative air humidity (%). The resulting regression equation is as follows:

$$Y = a\,X1 + b\,X2 + c\,X3 + d \quad (8)$$

The analysis of the dependence of meteorological parameters on the resulting *NDVI* is presented in Section 3.5.2.

To account for potential nonlinear relationships between vegetation indices and environmental variables, spline-based regression functions were additionally applied. This approach is conceptually equivalent to a Generalized Additive Model (GAM), enabling the detection of nonlinear trends while preserving model interpretability.

3. Results

3.1. Agro-Climatic Conditions During the Monitoring Period

The agro-climatic data for 2024 are presented in Figure 4 and those for 2025 in Figure 5. Both observation periods were characterized by anomalously elevated air temperatures and below-average precipitation totals, which resulted in the reduced relative humidity of air throughout most of the vegetation cycle.

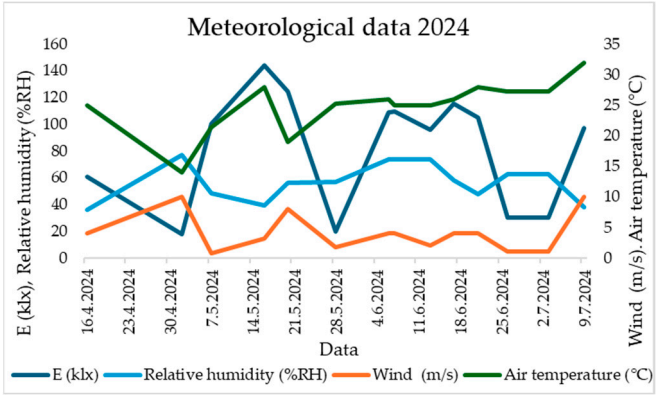


Figure 4. Weather conditions during the 2024 experiments.

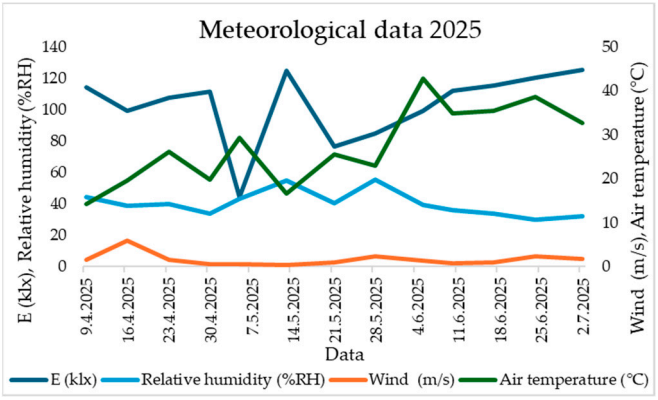


Figure 5. Weather conditions during the 2025 experiments.

3.2. Soil Parameters During Measurement

The measured soil parameters obtained using the USB portable soil detector for the 2025 season are shown in Table 1.

Table 1. Soil parameters measured during the 2025 triticale growing season.

No	Date	Time	Soil Temp (°C)	Moisture (%)	Conductivity (us/cm)	pH	N (mg/kg)	P (mg/kg)	K (mg/kg)	Fertility (mg/kg)
1	27.3 2025	14:16	18.9	18.9	117.0	6.7	5	8	18	64
2	9.4 2025	13:04	14.9	31.5	291.0	6.3	14	20	46	160
3	16.4 2025	13:18	21.4	22.2	163.0	6.3	8	11	26	89
4	23.4 2025	12:57	26.5	20.3	132.0	6.3	6	9	21	72
5	30.4 2025	13:03	25.4	20.8	238.0	6.4	11	16	38	130
6	5.5 2025	10:56	23.0	23.1	221.0	6.2	11	15	35	121
7	13.5 2025	13:53	21.9	21.7	258.0	6.2	12	18	41	141
8	21.5 2025	13:19	26.9	23.5	269.0	6.3	13	18	43	147
9	28.5 2025	12:30	21.8	14.2	128.0	6.3	6	8	20	70
10	5.6 2025	14:46	35.7	22.0	185.0	6.2	9	12	29	101
11	10.6 2025	13:59	30.5	10.3	60.0	7.0	3	4	9	33
12	17.6 2025	13:26	30.8	16.1	63.0	6.5	3	4	10	34
13	24.6 2025	13:00	39.0	10.2	8.0	7.0	0	0	1	4
14	9.7 2025	16:35	45.3	4.6	0.0	7.0	0	0	0	0

The anomalously high air and soil temperatures combined with low relative humidity observed in late May and early June 2025 (Figure 5, Table 1) likely induced physiological stress in triticale plants, including stomatal closure, reduced transpiration, and the inhibition of photosynthesis [28]. Soil temperature increased sharply from 21.8 °C on 28 May to 35.7 °C on 5 June, accompanied by a decrease in soil moisture and relative air humidity.

These stress responses directly influenced the spectral vegetation indices, resulting in the observed earlier peak of NDVI, SAVI, EVI2, and NIRI in 2025. The integration of meteorological and soil data with the spectral indices allows for a more detailed interpretation of stress-induced vegetation dynamics, highlighting the sensitivity of triticale to short-term heat and drought events.

This analysis demonstrates that the observed changes in vegetation indices are not merely correlated with general weather conditions but are linked to specific physiological responses of the plants under regional agro-climatic conditions, providing a more comprehensive understanding of vegetation dynamics in the southern Dobruja region.

Soil samples were collected simultaneously with each UAV flight, allowing for direct comparison between soil parameters and the corresponding spectral vegetation indices.

3.3. Field Data

Figure 6 illustrates the main stages of crop development, presented visually to facilitate the identification of phenological phases.



Figure 6. Stages of crop development.

The phenological stages illustrated in Figure 6 serve as a common temporal reference for interpreting the vegetation index time series. While absolute index values differ among varieties, the relative timing of index peaks and declines was consistently evaluated in relation to these phenological phases rather than absolute magnitude alone.

Sowing in 2024 was conducted on 29 April for varieties *17/5* and *20/52* and on 2 May for varieties *22/78*, *22/71*, and *Kolorit*. Emergence was recorded on 15 April 2024, tillering on 10 May, and stem elongation (grading) on 31 May. The initial plant height by experimental plot is presented in Table 2.

Table 2. Initial plant height by plot on 17 July 2024 (cm).

	I	II	III	IV	V
5	90–97	85–92	70–90	65–75	80–85
4	80–95	90–100	85–100	65–75	70–75
3	90–95	90–95	82–87	65–70	70–80
2	90–95	85–90	85–90	80–85	75–80
1	85–100	90–98	85–90	70–75	70–75

Sowing in 2025 was conducted on 27 March for all experimental plots. Emergence was recorded on 9 April 2025, tillering on 3 May, and heading on 1 June. The initial plant height by plot is presented in Table 3.

Table 3. Initial plant height by plot on 17 July 2025 (cm).

	I	II	III	IV	V
3	100–117	92–117	90–96	86–96	85–96
2	106–112	88–96	86–93	94–103	94–96
1	94–106	90–106	82–96	82–92	90–92

3.4. Vegetation Indices

The *Kolorit* variety is characterized by highly stable temporal dynamics of the spectral vegetation indices, which makes it suitable for use as a reference genotype in comparative remote-sensing analyses. In 2024 (Figure 7), the NDVI trajectory shows a steady increase from low initial values in mid-April to a well-defined maximum in late May when the index exceeds 0.60. The smooth progression reflects uniform crop development, expressed through the consistent accumulation of green biomass and gradual canopy closure. During the period of maximum values, a distinct plateau is observed, indicating an extended phase of intensified and sustained photosynthetic activity. After this stage, the NDVI values gradually decline, corresponding to the onset of grain filling and subsequent leaf senescence.

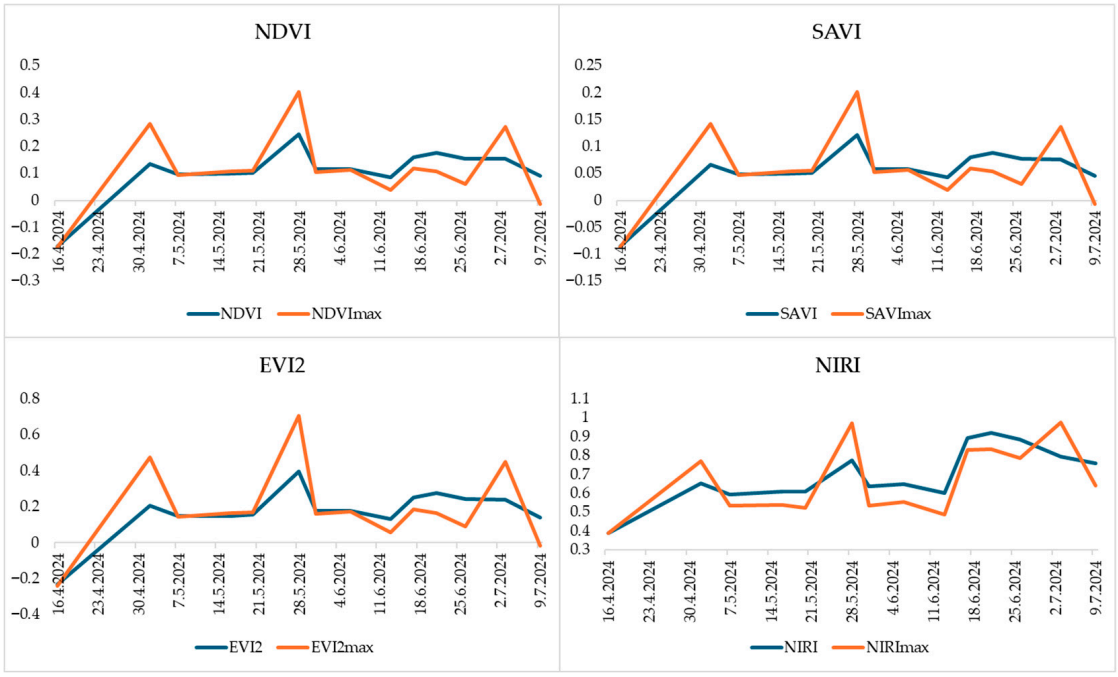


Figure 7. Temporal dynamics of NDVI, SAVI, EVI2, and NIRI for the *Kolorit* variety measured in 2024.

The dynamics of the SAVI exhibit a similar pattern, with values being more stable and less affected by soil background reflectance during the early vegetative stages. This stability enables a more accurate assessment of canopy cover at the onset of tillering. The EVI2 demonstrates a pronounced peak exceeding 0.70, which coincides with the active tillering phase. A characteristic feature of *Kolorit* is the abrupt transition between phenological stages: the EVI2 curve increases sharply but maintains its maximum value over an extended period, indicating prolonged high photosynthetic efficiency. The NIRI dynamics further confirm this stability, reaching values above 0.80 at the end of May and gradually decreasing throughout June.

In 2025 (Figure 8), the temporal dynamics of the spectral indices followed a similar pattern to 2024, but the maxima were attained earlier: mid-May. This shift is attributed to the higher air temperatures and reduced soil and atmospheric moisture, which accelerated

phenological development. Despite the earlier occurrence of the peaks, *Kolorit* maintained relatively high values across all indices compared to the other varieties, with the NIRI exhibiting the slowest rate of decline. These observations indicate stable physiological activity of the leaf apparatus even under stress conditions. Accordingly, *Kolorit* can be characterized as a variety with high adaptability and the most stable spectral profile among the tested genotypes.

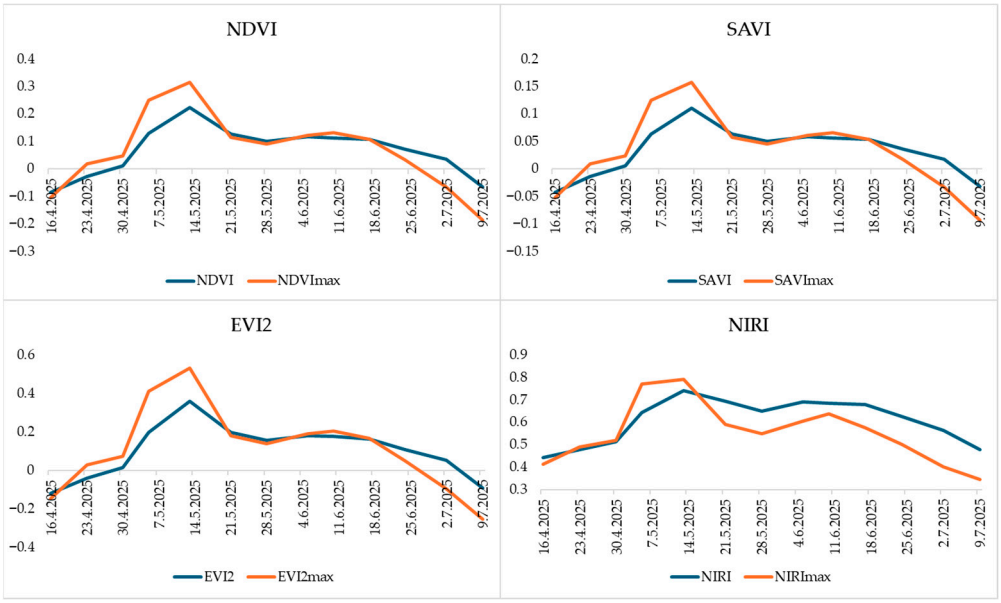


Figure 8. Temporal dynamics of NDVI, SAVI, EVI2, and NIRI for the *Kolorit* variety measured in 2025.

Variety *17/5* exhibits a spectral index temporal dynamics pattern similar to that of *Kolorit*, but with substantially lower values and a shorter phase of maximum photosynthetic activity. In 2024 (Figure 9), the NDVI increases from negative values in early April; however, the curve rises more gradually and reaches its peak approximately one week later. The maximum value, around 0.55, is markedly lower than that of *Kolorit*, indicating reduced green biomass accumulation and lower canopy density. Following the peak, the NDVI declines more rapidly, suggesting an earlier onset of the senescence phase.

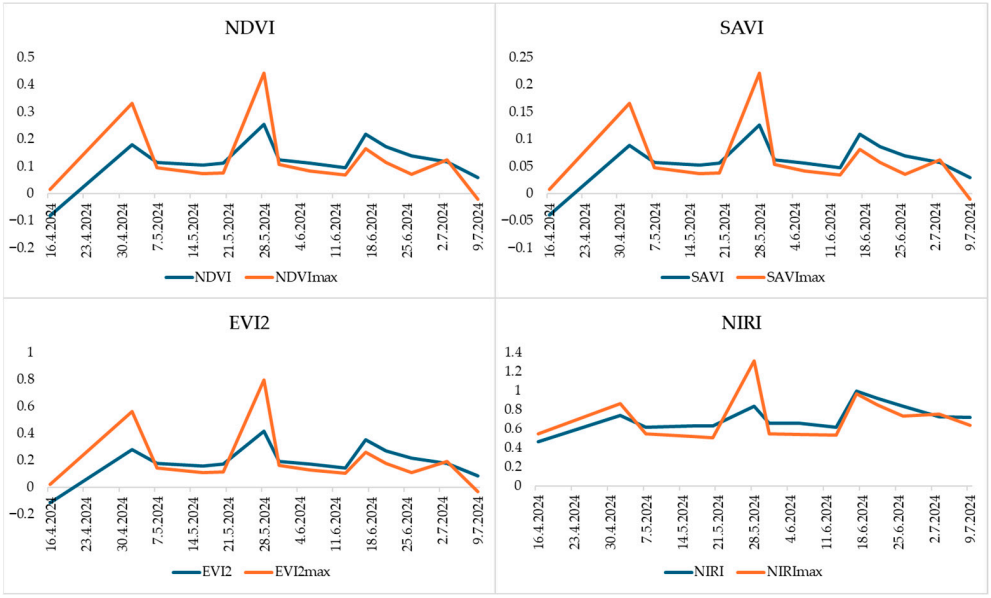


Figure 9. Temporal dynamics of NDVI, SAVI, EVI2, and NIRI for variety *17/5* measured in 2024.

The SAVI confirms these observations, with values remaining below those of *Kolorit* throughout the growing season, with the largest differences observed in early May. The EVI2 curve for variety *17/5* displays a gentler slope during the ascending phase and attains a lower maximum compared to the reference variety, reflecting reduced photosynthetic efficiency and a shorter period of active photosynthesis. The NIRI further emphasizes this pattern, with values beginning to decline earlier, in early June, indicating accelerated leaf senescence.

In 2025 (Figure 10), variety *17/5* exhibited increased sensitivity to adverse environmental conditions. The NDVI reached its maximum in early May, but with values lower than those of *Kolorit*, followed by a rapid decline. SAVI and EVI2 showed similar patterns, with lower maxima and steeper descending trajectories. The NIRI exhibited an early and pronounced decrease, reflecting the variety's limited physiological resilience. Overall, variety *17/5* is characterized by reduced stability and an earlier onset of senescence compared to the reference variety, placing it among the genotypes most sensitive to water and temperature stress.

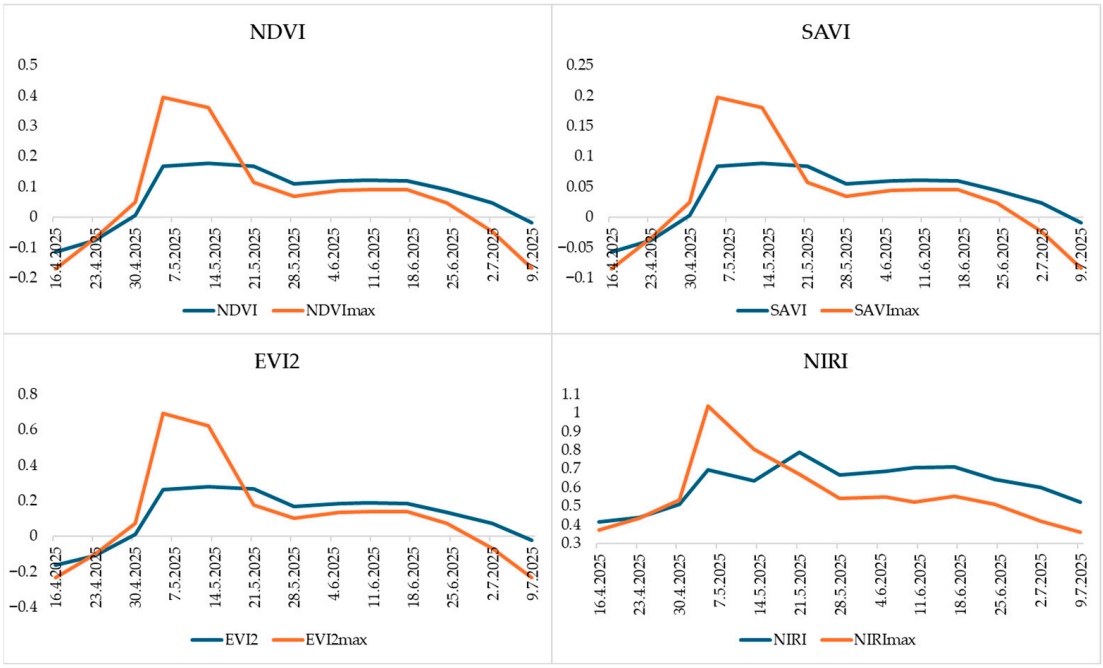


Figure 10. Temporal dynamics of NDVI, SAVI, EVI2, and NIRI for variety *17/5* measured in 2025.

Variety *20/52* is characterized by high spectral index values, particularly in 2024 (Figure 11), when it exceeds *Kolorit* in both maximum values and the duration of the active vegetation phase. The NDVI for this variety surpasses 0.65 at the end of May, indicating an exceptionally high canopy density and intensive accumulation of green biomass. The SAVI also exhibits elevated values, especially during the tillering period, when plants reach the peak of physiological activity. The EVI2 highlights the variety's advantage, attaining maximum values above 0.75 and maintaining a stable plateau for several weeks. This pattern reflects an extended phase of high photosynthetic efficiency, distinguishing *20/52* from the other varieties. The NIRI confirms these observations, showing high values and a slower rate of decline throughout June. Collectively, these characteristics suggest that the variety has strong potential for high productivity under favorable climatic conditions and adequate resource availability.

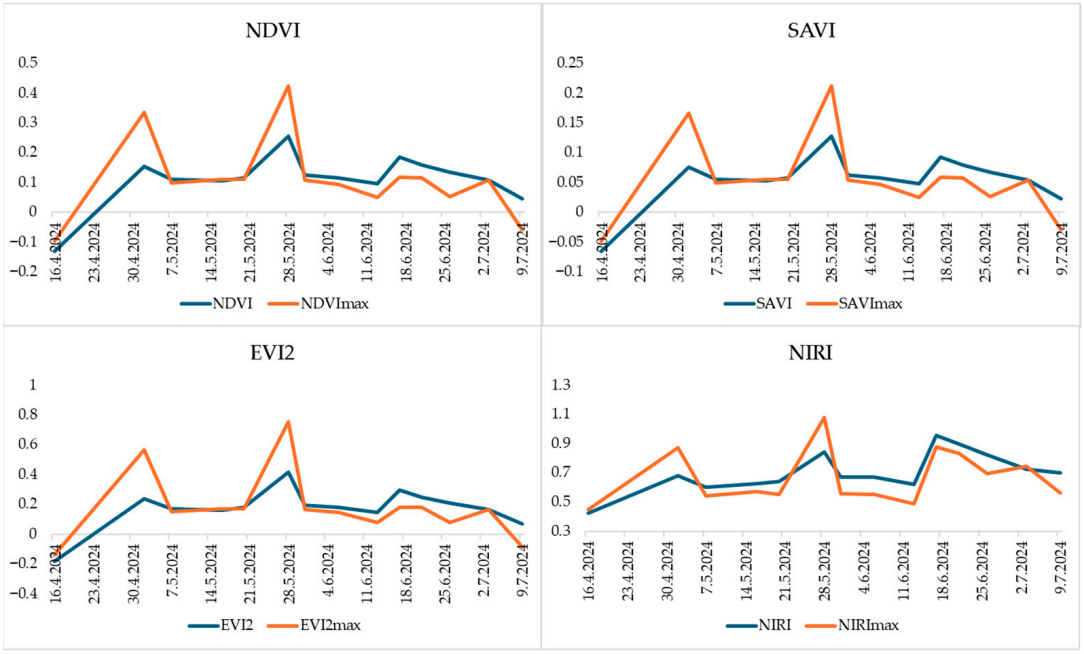


Figure 11. Temporal dynamics of NDVI, SAVI, EVI2, and NIRI for variety *20/52* measured in 2024.

In 2025 (Figure 12), the temporal dynamics of spectral indices for variety *20/52* exhibited notable changes. NDVI and SAVI reached their maxima earlier and at lower values than in the previous year, followed by a steeper decline, indicating accelerated crop senescence. EVI2, while still displaying a pronounced peak, showed a reduced amplitude and shorter duration of maximum activity. The NIRI demonstrated better retention of values compared to some other varieties but also began to decline earlier than in 2024. Compared with *Kolorit*, variety *20/52* performs well under favorable conditions but exhibits a greater sensitivity to stress, characterizing it as highly productive yet less stable.

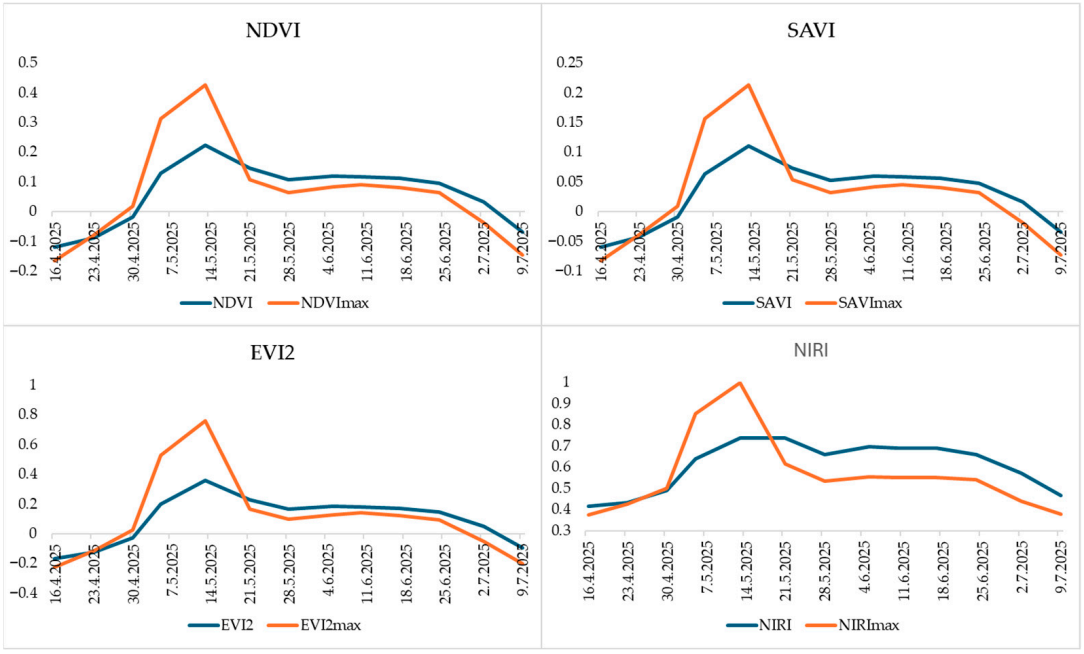


Figure 12. Temporal dynamics of NDVI, SAVI, EVI2, and NIRI for variety *20/52* measured in 2025.

Variety *22/78* exhibits markedly slower growth and lower spectral index values compared to *Kolorit*. In 2024 (Figure 13), the NDVI increased gradually, reaching its maximum only in early June, with values approximately 10–15% lower than those of the reference variety. This pattern reflects limited green biomass accumulation and reduced canopy density. The SAVI mirrors this trend, displaying a smooth curve with lower amplitude.

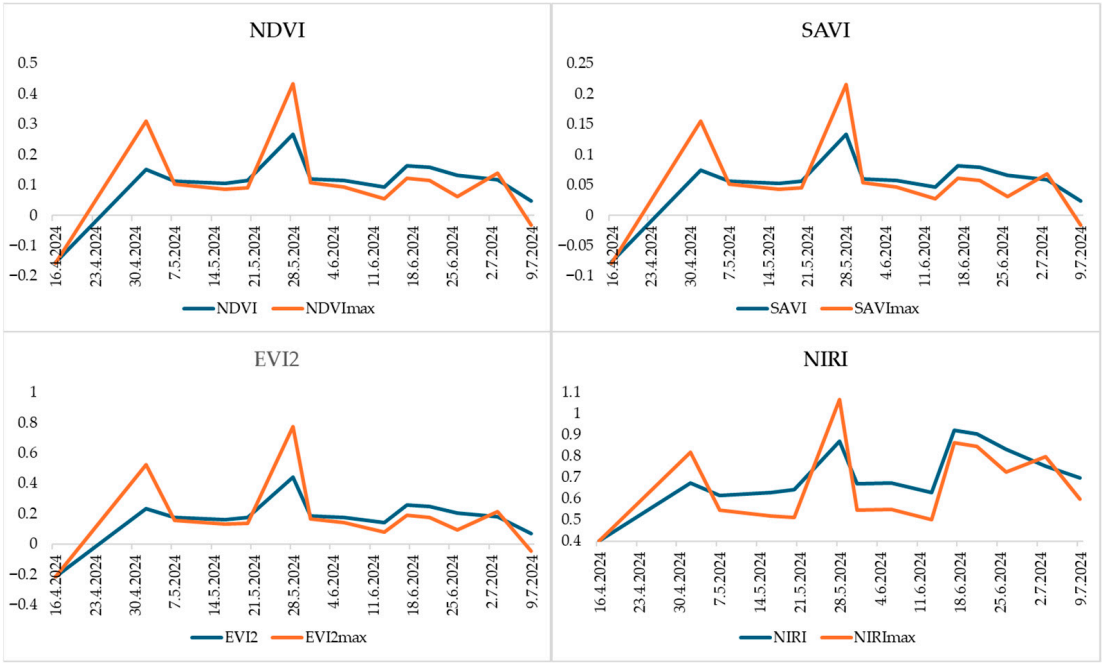


Figure 13. Temporal dynamics of NDVI, SAVI, EVI2, and NIRI for variety *22/78* measured in 2024.

The EVI2 for *22/78* shows a less pronounced peak, indicating reduced photosynthetic efficiency. The absence of a clear plateau in maximum values suggests a short and limited period of high photosynthetic activity. The NIRI confirms this pattern, with values beginning to decline relatively early, already by the end of May. Collectively, these observations indicate that the variety has a shorter period of active physiological growth and undergoes earlier leaf senescence.

In 2025 (Figure 14), these characteristics became even more pronounced. The NDVI reached a lower maximum and declined sharply after mid-May. The SAVI remained at low values throughout the season, and the EVI2 did not exhibit a distinct peak, indicating markedly reduced photosynthetic activity. The NIRI declined more rapidly, reflecting accelerated leaf senescence. Compared with *Kolorit*, variety *22/78* exhibited substantially lower stability and greater sensitivity to adverse environmental conditions, characterizing it as the most vulnerable of the studied varieties.

Variety *22/71* occupies an intermediate position between *Kolorit* and the other tested varieties. In 2024 (Figure 15), the NDVI indicates a more rapid increase during the early vegetative stages, reaching values close to those of *Kolorit*; however, the maximum occurs earlier. This pattern suggests intensive initial growth, which may provide an advantage under short and cooler spring conditions. The SAVI confirms this behavior, with its curve rising earlier and already attaining high values in early May. The EVI2 exhibits a distinct peak comparable to that of *Kolorit*, although the subsequent decline is steeper, indicating a shorter duration of the high photosynthetic activity phase. The NIRI shows a similar dynamic, with a rapid increase at the beginning, followed by an earlier decline compared to the reference variety. Overall, in 2024, variety *22/71* can be characterized by vigorous initial growth but a shorter duration of the active vegetation phase.

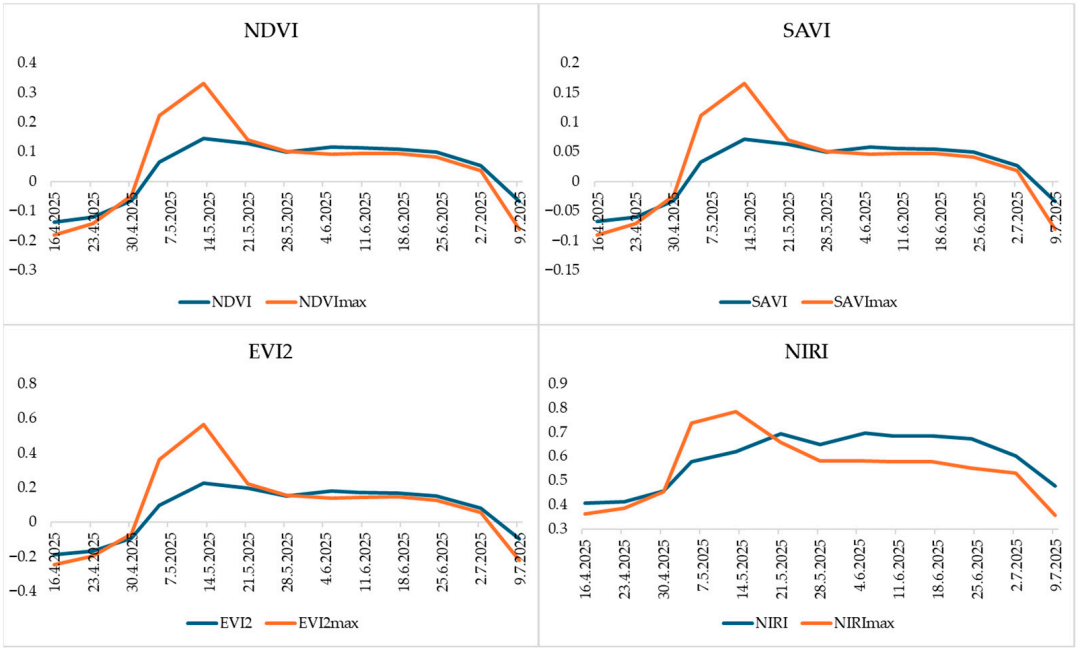


Figure 14. Temporal dynamics of NDVI, SAVI, EVI2, and NIRI for variety *22/78* measured in 2025.

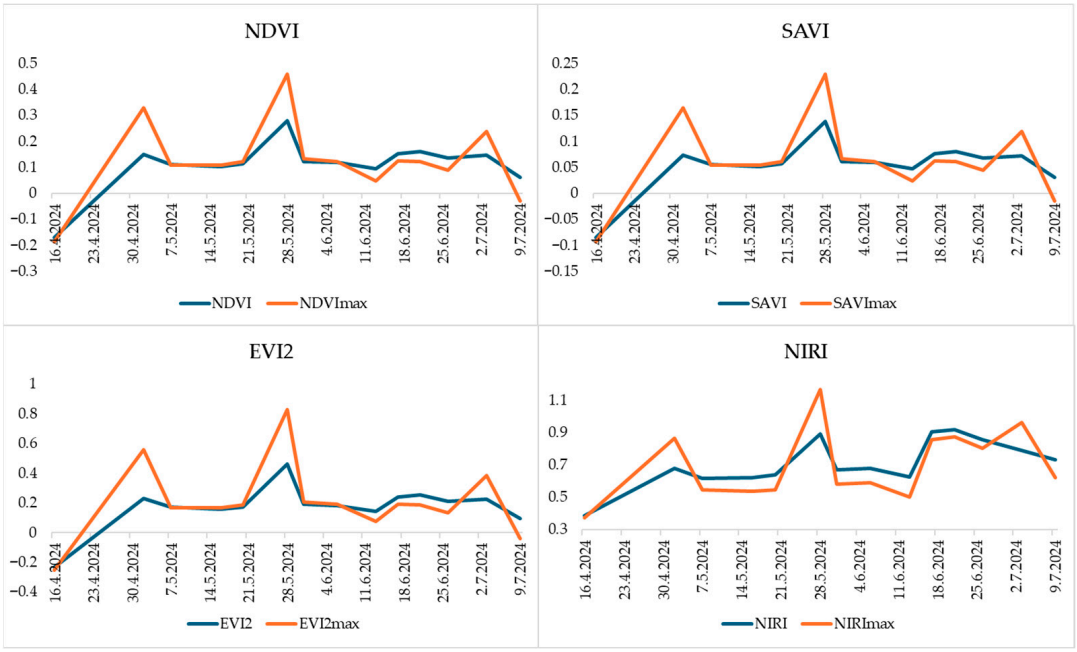


Figure 15. Temporal dynamics of NDVI, SAVI, EVI2, and NIRI for variety *22/71* measured in 2024.

In 2025 (Figure 16), the differences with respect to *Kolorit* became more pronounced. The NDVI reached its maximum as early as May, although the values were lower. The decline occurred more rapidly, indicating a greater sensitivity to stress conditions. Both the SAVI and EVI2 exhibited earlier and lower peaks. The NIRI already showed a marked decrease in late May, which shortened the period of active physiological growth. Compared to *Kolorit*, variety *22/71* displayed stronger dynamics during the initial phases but reduced stability in the later stages, placing it in an intermediate position regarding adaptability and resilience.

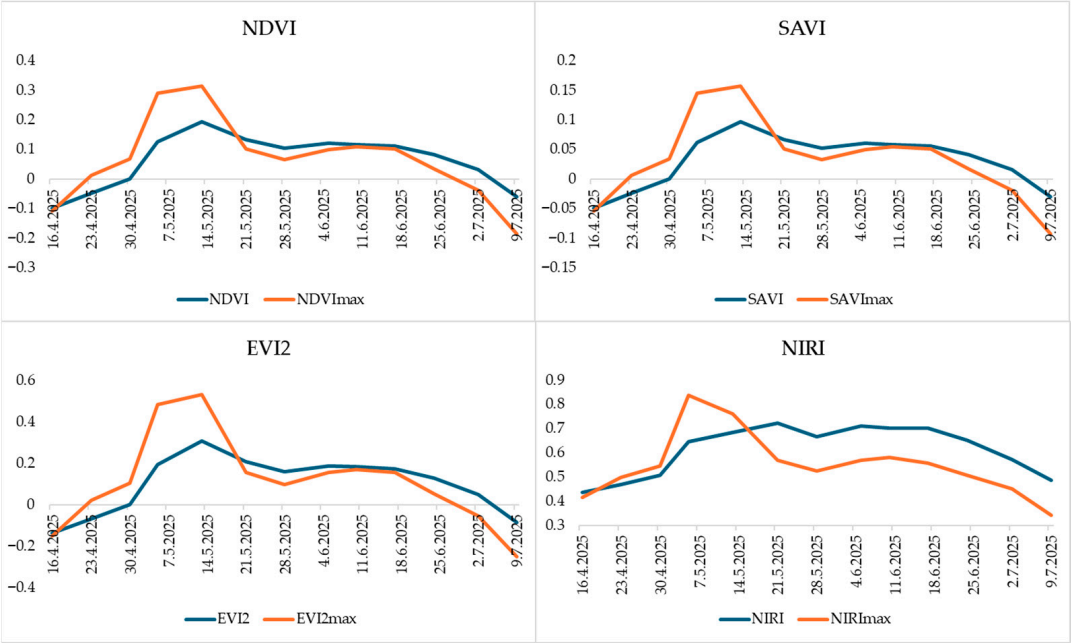


Figure 16. Temporal dynamics of NDVI, SAVI, EVI2, and NIRI for variety *22/71* measured in 2025.

The detailed characterization of spectral indices reveals clear distinctions among the varieties. *Kolorit* is characterized by stable dynamics, smooth index curves, and a prolonged period of high physiological activity. Variety *17/5* exhibits lower amplitudes and earlier senescence, rendering it more sensitive. Variety *20/52* demonstrates the highest index values and an extended phase of activity in 2024 but shows greater vulnerability in 2025. Variety *22/78* displays the lowest physiological efficiency and a short active phase, whereas *22/71* shows an advantage during early developmental stages but a faster decline in activity in later phases. The soil and climatic conditions in 2025 act as a common background factor, accelerating phenological development and shortening the period of maximum photosynthetic activity in all varieties, albeit to varying degrees of intensity.

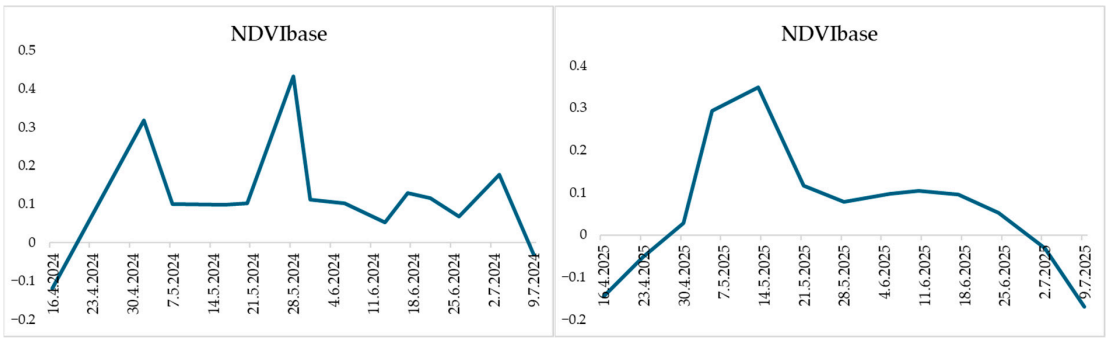
Although the temporal dynamics of the vegetation indices are presented separately for clarity, the comparative analysis reveals three distinct groups of varieties characterized by different spectral response profiles: (1) a stable and stress-resilient variety (*Kolorit*), (2) a high-productivity but stress-sensitive variety (*20/52*), and (3) early-senescing or physiologically constrained varieties (*17/5*, *22/78*, and partially *22/71*). This grouping provides an integrated interpretation of the multi-index time-series results.

3.5. Analysis of the Temporal Dynamics of NDVI

3.5.1. Analysis of NDVI Deviations from the Mean Trend

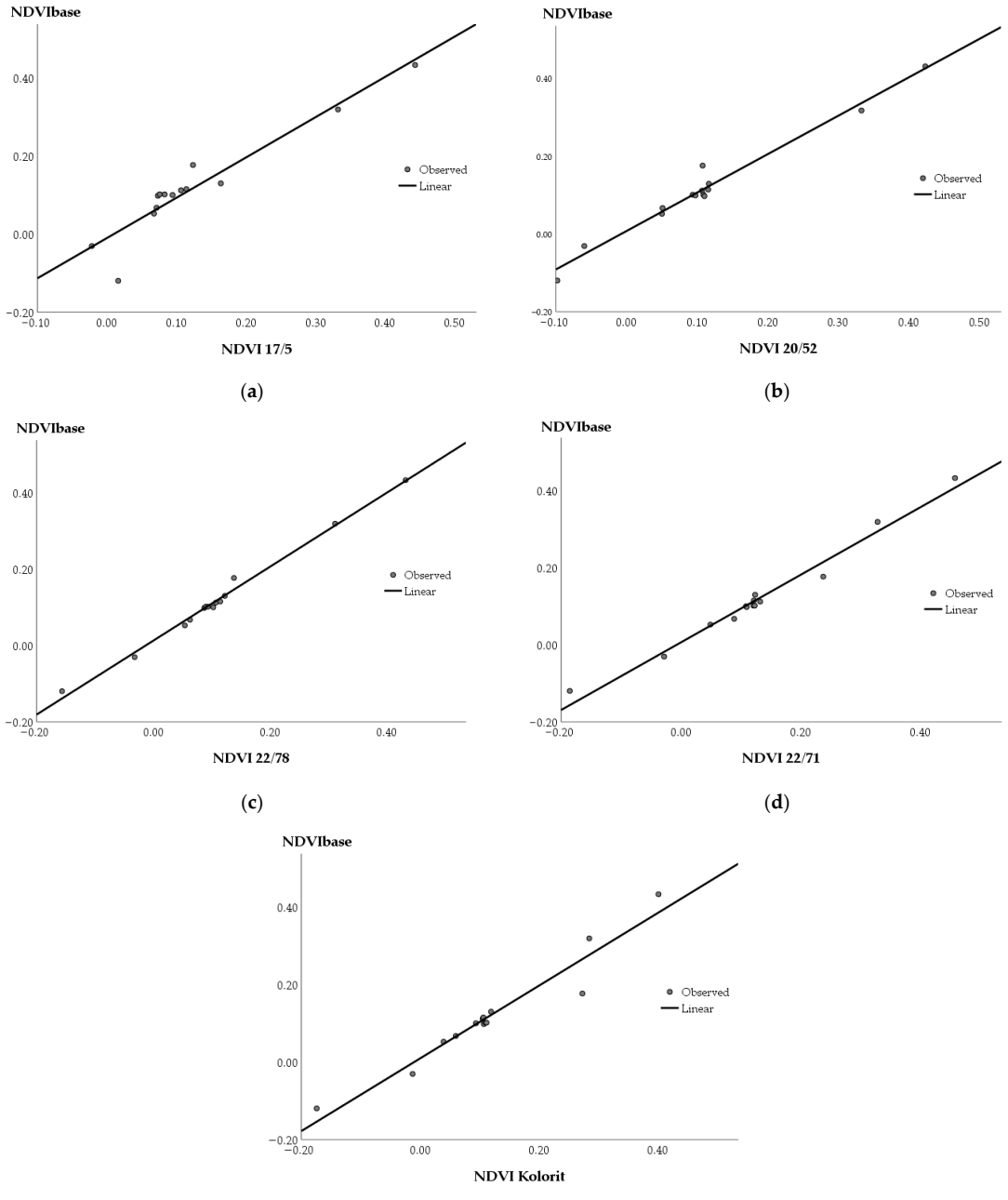
The expected value of the NDVIbase for each growing season was calculated using Equation (6). For the 2024 season, it is presented in Figure 17a, and for the 2025 season, it is presented in Figure 17b. The resulting dynamics of the NDVIbase changes reflect the specific characteristics of each season. These are consistent with the climatic and soil conditions during the vegetation period, as shown in Figures 4 and 5 and Table 1.

Figure 18 illustrates the varietal trends relative to the baseline NDVIbase for the 2024 season, and the corresponding correlation relationships are summarized in Table 4. The table indicates the degree of overlap between the expected baseline values and the observed NDVI dynamics of individual varieties. Variety *22/71* shows the highest correspondence with the NDVIbase trajectory, whereas variety *17/5* exhibits the least overlap, indicating that its temporal dynamics deviate most from the expected pattern.



(**a**) (**b**)

Figure 17. NDVIbase for the 2024 season (**a**) and for the 2025 season (**b**).



(**a**) (**b**)

(**c**) (**d**)

(**e**)

Figure 18. NDVI dependence by variety relative to NDVIbase for the 2024 season: variety *17/5* (**a**), variety *20/52* (**b**), variety *22/78* (**c**), variety *22/71* (**d**), and variety *Kolorit* (**e**).

Table 4. Correlations for the 2024 season.

		NDVIbase	NDVI 17/5	NDVI 20/52	NDVI 22/78	NDVI 22/71	NDVI Kolorit
Pearson Correlation	NDVIbase	1.000	0.946	0.986	0.996	0.989	0.968
	NDVI 17/5	.	1.000	0.960	0.938	0.891	0.851
	NDVI 20/52	.	.	1.000	0.986	0.957	0.919
	NDVI 22/78	.	.	.	1.000	0.984	0.956
	NDVI 22/71	.	.	.	.	1.000	0.990
	NDVI Kolorit	.	.	.	.	.	1.000

For variety *17/5*, the correspondence with NDVIbase is R = 0.946, R^2 = 0.896, and Adjusted R^2 = 0.887 (Figure 18a; Table 4), representing the most distinct deviation from the baseline trend. Varieties *20/52*, *22/78*, *22/71*, and *Kolorit* show R^2 values of 0.972, 0.992, 0.978, and 0.937, respectively, indicating varying degrees of alignment with the expected seasonal values (Figure 18b–e; Table 4).

Varietal trends relative to the baseline for the 2025 season are presented in Figure 19, with the corresponding correlation relationships summarized in Table 5.

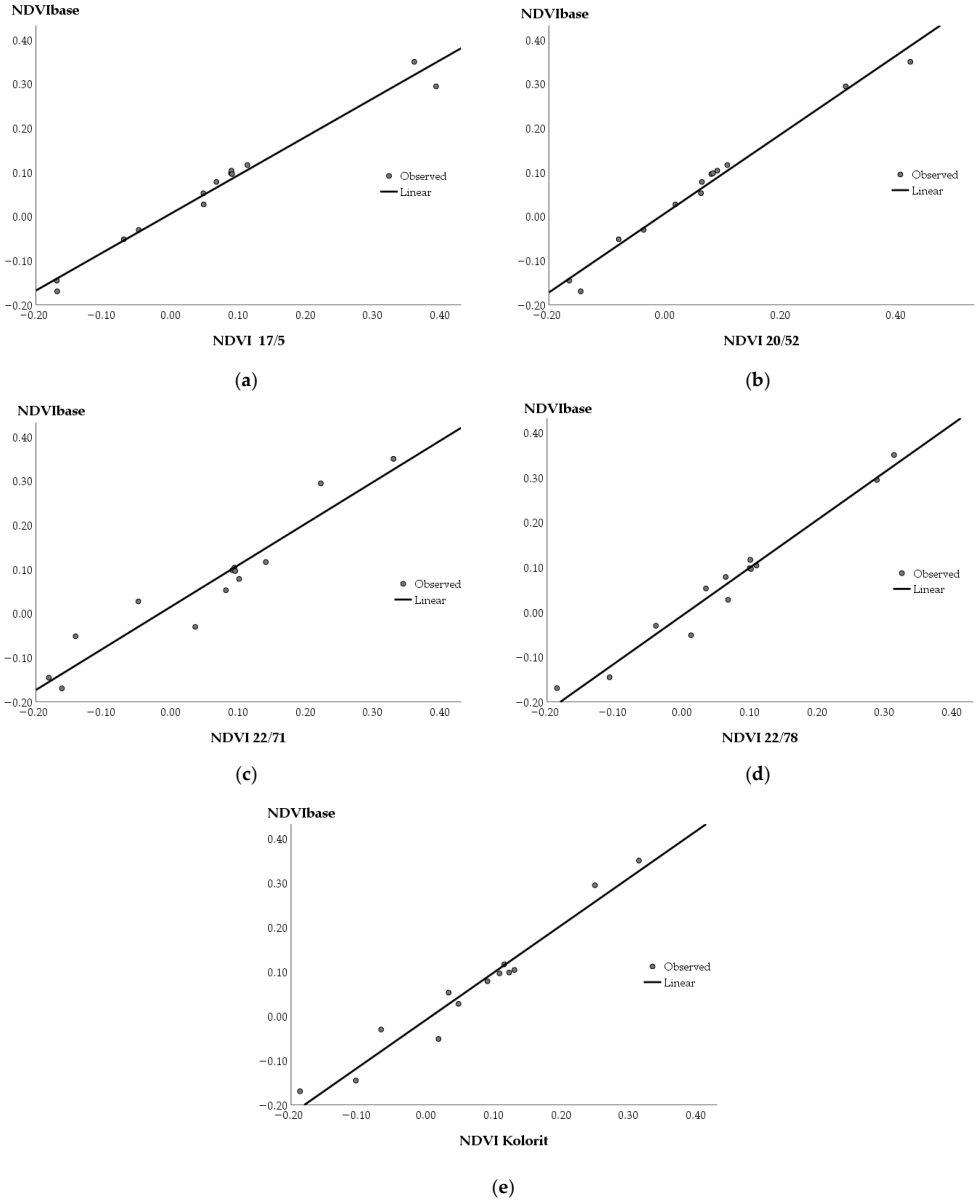


Figure 19. NDVI dependence by variety relative to NDVIbase for the 2025 season: variety *17/5* (**a**), variety *20/52* (**b**), variety *22/71* (**c**), variety *22/78* (**d**), and variety *Kolorit* (**e**).

Table 5. Correlations for the 2025 season.

		NDVIbase	NDVI 17/5	NDVI 20/52	NDVI 22/78	NDVI 22/71	NDVI Kolorit
Pearson Correlation	NDVIbase	1.000	0.988	0.990	0.953	0.983	0.975
	NDVI 17/5	.	1.000	0.981	0.920	0.975	0.952
	NDVI 20/52	.	.	1.000	0.950	0.960	0.947
	NDVI 22/78	.	.	.	1.000	0.891	0.893
	NDVI 22/71	.	.	.	.	1.000	0.990
	NDVI Kolorit	.	.	.	.	.	1.000

The correspondence of variety *17/5* with NDVIbase is R = 0.988, R^2 = 0.977, and Adjusted R^2 = 0.974 (Figure 19a; Table 5). For variety *20/52*, R = 0.990, R^2 = 0.981, and Adjusted R^2 = 0.979 (Figure 19b; Table 5), indicating that its value is closest to the expected seasonal value. For variety *22/78*, R = 0.953, R^2 = 0.908, and Adjusted R^2 = 0.899 (Figure 19c), which is clearly visible in the graph and represents the most distinct deviation from the baseline trend. For variety *22/71*, R = 0.983, R^2 = 0.967, and Adjusted R^2 = 0.964 (Figure 19d). For variety *Kolorit*, R = 0.975, R^2 = 0.952, and Adjusted R^2 = 0.947 (Figure 19e).

Table 5 presents the degree of correspondence between the temporal NDVI trends of the remaining varieties and the typical NDVIbase values for the 2025 season. The data indicate that variety *20/52* shows the highest agreement with the NDVIbase trajectory, while variety *22/78* exhibits the lowest, reflecting the greatest deviation from the expected seasonal pattern.

3.5.2. Regression Analysis

The results of the regression analysis of NDVI variety *Kolorit* (Y) assessing the influence of the following environmental parameters—X_1: soil moisture (%), X_2: air temperature (°C), and X_3: relative air humidity (%)—are presented in Table 6.

Table 6. Descriptive statistics.

	Mean	Std. Deviation	N
NDVI	0.0787	0.13589	12
Moisture	16.5833	6.25501	12
Air temperature	28.6667	8.28211	12
Relative humidity	39.6333	8.14687	12

The Pearson correlation relationships are presented in Table 7. The results indicate that the dependence of the NDVI on air temperature is relatively low, whereas the correlations with soil moisture and relative air humidity are 43.9% and 56.2%, respectively. Soil moisture exhibits a direct effect on crop development, while relative air humidity not only influences vegetation but also affects the accuracy of reflected solar radiation measurements.

Table 7. Correlations.

		NDVI	Moisture	Air Temperature	Relative Humidity
Pearson Correlation	NDVI	1.000	0.439	−0.097	0.562
	Moisture	0.439	1.000	−0.670	0.399
	Air temperature	−0.097	−0.670	1.000	−0.554
	Relative humidity	0.562	0.399	−0.554	1.000
Sig. (1-tailed)	NDVI	.	0.077	0.383	0.029
	Moisture	0.077	.	0.009	0.099
	Air temperature	0.383	0.009	.	0.031
	Relative humidity	0.029	0.099	0.031	.

The multiple regression coefficient (R) was 0.781, indicating a satisfactory level of predictive capability. The coefficient of determination (R^2), representing the proportion of variance in the dependent variable explained by the independent variables, accounted for 61.0% of the variability. A summary of the regression analysis is presented in Table 8.

Table 8. Model Summary [a].

Model	R	R Square	Adjusted R Square	Std. Error of the Estimate	Change Statistics					Durbin-Watson
					R Square Change	F Change	df1	df2	Sig. F Change	
1	0.781 [a]	0.610	0.464	0.09952	0.610	4.169	3	8	0.047	1.477

[a] Predictors: (constant), Relative_humidity, moisture, Air_temperature; Dependent aariable: NDVI.

The F statistic evaluates the overall fit of the regression model. The results show that the independent variables significantly predict the dependent variable, F (3, 8) = 4.169, p = 0.047, confirming that the model reliably explains the variability in the dependent variable. The statistical significance of the ANOVA regression is summarized in Table 9.

Table 9. ANOVA [a].

Model		Sum of Squares	df	Mean Square	F	Sig.
1	Regression	0.124	3	0.041	4.169	0.047 [b]
	Residual	0.079	8	0.010		
	Total	0.203	11			

[a] Dependent variable: NDVI; Predictors: (constant), Relative_humidity, moisture, and Air_temperature. [b] Predictors: (Constant).

The correlation and covariance coefficients of the three predictors with respect to the NDVI are presented in Table 10.

Table 10. Coefficient correlations [a].

Model			Relative_Humidity	Moisture	Air_Temperature
1	Correlations	Relative_humidity	1.000	−0.045	0.422
		Moisture	−0.045	1.000	0.588
		Air_temperature	0.422	0.588	1.000
	Covariances	Relative_humidity	1.963×10^{-5}	-1.278×10^{-6}	1.006×10^{-5}
		Moisture	-1.278×10^{-6}	4.184×10^{-5}	2.048×10^{-5}
		Air_temperature	1.006×10^{-5}	2.048×10^{-5}	2.897×10^{-5}

[a] Dependent variable: NDVI.

Residuals statistics are presented in Table 11.

Table 11. Residuals statistics [a].

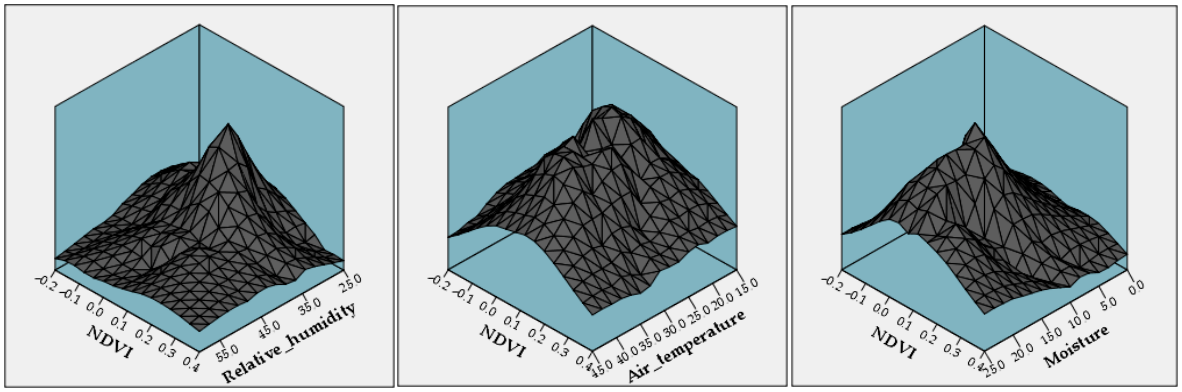
	Minimum	Maximum	Mean	Std. Deviation	N
Predicted Value	−0.1343	0.2171	0.0787	0.10612	12
Residual	−0.13847	0.13230	0.00000	0.08487	12
Std. Predicted Value	−2.008	1.304	0.000	1.000	12
Std. Residual	−1.391	1.329	0.000	0.853	12

[a] Dependent variable: NDVI.

The unstandardized coefficients represent the change in the dependent variable per unit change in each independent variable, holding all others constant. The regression equation for predicting the NDVI is therefore expressed as:

$$Y = 0.014\ X1 + 0.012\ X2 + 0.012\ X3 - 0.963 \quad (9)$$

Figure 17 illustrates the relationships between the NDVI and examined predictors. Specifically, NDVI dependence on relative air humidity, air temperature, and soil moisture is shown in Figure 20a and 20b, and 20c, respectively.



(**a**) (**b**) (**c**)

Figure 20. NDVI dependence on environmental variables: (**a**) relative air humidity, (**b**) air temperature, and (**c**) soil moisture.

4. Discussion

This study represents the first detailed temporal analysis of spectral vegetation indices for triticale varieties in the Southern Dobruja region. Over two growing seasons, the dynamics of the NDVI, SAVI, EVI2, and NIRI were monitored, providing a comprehensive dataset for varietal evaluation and the creation of a reference database. The applicability of the NIRI for remote phenotyping and variety differentiation was specifically examined [23].

The results demonstrate that spectral vegetation indices are reliable indicators for varietal discrimination when analyzed as temporal dynamics rather than single-date measurements. Aggregated descriptors derived from the NDVI, SAVI, EVI2, and NIRI curves significantly enhanced differentiation among the five triticale varieties, consistent with studies in rice, soybean, and maize, where seasonal index signatures showed stronger correlations with physiological traits and yield [29–31].

Among the indices, the NDVI and SAVI exhibited limited specificity due to sensitivity to soil background and climatic variability [20]. In contrast, NIRI and EVI2 provided the most informative and consistent profiles, capturing varietal-specific physiological behavior across the growing season. Integration with meteorological and soil data revealed that relative air humidity and soil moisture were key drivers of NDVI variability, highlighting the necessity of combining environmental parameters with spectral indices for accurate phenotypic assessment [32].

Varietal differences were evident in both years. *Kolorit* displayed stable spectral profiles with prolonged photosynthetic activity, indicating high adaptability and resilience. Variety *20/52* achieved the highest indices in 2024 but was more sensitive to environmental stress in 2025, illustrating the trade-off between high productivity and stress tolerance, consistent with findings in soybean [33]. Varieties *17/5* and *22/78* exhibited lower peaks and earlier senescence, reflecting reduced physiological efficiency and greater vulnerability to heat and drought, in line with studies in rice [34]. Variety *22/71* showed rapid early growth but

a shorter active vegetation phase, representing an intermediate phenotype analogous to early-maturing genotypes in other crops [30].

Climatic variations between seasons had pronounced effects. Elevated temperatures and reduced humidity in late May and early June 2025 accelerated phenological development, producing earlier peaks and faster declines in all indices. Physiological mechanisms likely included stomatal closure, reduced transpiration, and the inhibition of photosynthesis, linking environmental stress to observed spectral changes. These findings underscore the importance of interpreting vegetation indices within the context of regional agroclimatic conditions rather than in isolation.

The methodology used in this study is practically applicable for breeding programs and agricultural management in Southern Dobruja. Identification of the most informative indices (NIRI and EVI2) provides a quantitative basis for optimizing phenotyping strategies. The observed varietal responses enable breeders to select or develop triticale varieties adapted to the specific climatic conditions of the region, while farmers can use this information to plan agronomic interventions such as irrigation timing or stress mitigation measures.

Overall, the results confirm that spectral indices act as a phenotypic fingerprint of the genotype, integrating genetic and environmental influences. *Kolorit* is distinguished by stability and adaptability, *20/52* by high productivity potential with moderate stress sensitivity, and *17/5* and *22/78* by earlier senescence and reduced physiological efficiency. These insights demonstrate the potential of temporal multispectral monitoring as a robust, non-invasive tool for varietal evaluation and decision-making in breeding and crop management programs, supporting predictive phenotyping and adaptive agricultural practices [35].

By prioritizing temporal patterns and physiologically meaningful dynamics over single-date comparisons, the proposed framework bridges high-resolution UAV phenotyping with interpretable statistical modeling, offering a practical alternative to black-box machine learning approaches in small-plot breeding experiments.

5. Conclusions

This study demonstrates clear varietal-specific growth patterns and spectral vegetation index dynamics in five triticale (×*Triticosecale Wittm.*) varieties cultivated under the agroecological conditions of Southern Dobruja, Bulgaria, over two consecutive growing seasons. The temporal behavior of the NDVI, SAVI, EVI2, and NIRI enabled effective differentiation among varieties, with *Kolorit* exhibiting high physiological stability and prolonged vegetation activity, *20/52* showing high productivity potential but increased sensitivity to environmental stress, and varieties *17/5*, *22/78*, and *22/71* displaying shorter or less efficient vegetation phases.

From an applied breeding perspective, the results highlight the usefulness of multitemporal spectral indices as quantitative phenotypic markers for identifying genotypes with enhanced stress tolerance and adaptive capacity. The observed varietal responses provide practical guidance for breeders in selecting parental material suitable for the climatic conditions of Southern Dobruja, supporting the development of new triticale varieties with improved productivity and resilience.

For farmers and crop managers, the integration of UAV-based multispectral monitoring with meteorological and soil data offers a valuable decision-support tool. The identification of varieties with stable NDVI dynamics under heat and moisture stress can inform variety selection, optimize field management strategies, and reduce production risks under increasingly variable climatic conditions.

From a theoretical standpoint, the study contributes to a deeper understanding of genotype–environment interactions by demonstrating how spectral vegetation indices can serve as reliable indicators of plant physiological status under specific agro-climatic constraints. Among the indices analyzed, the NDVI and SAVI proved most suitable for the early-season screening of canopy development, while the EVI2 and NIRI were more responsive to environmental stress conditions, providing valuable markers for stress assessment.

Future research should expand this framework to a broader range of triticale genotypes, longer monitoring periods, and diverse agroecological regions. The integration of hyperspectral, thermal, and LiDAR data, combined with predictive modeling approaches, would further enhance phenotypic resolution and support the development of precision-oriented crop management and breeding strategies.

Author Contributions: Conceptualization, A.I.A. and H.P.S.; methodology, A.I.A. and H.P.S.; software, A.I.A. and H.P.S.; validation, A.I.A., H.P.S., A.Z.A. and B.I.E.; formal analysis, A.I.A. and H.P.S.; investigation, A.I.A. and H.P.S.; resources, A.I.A. and A.Z.A.; data curation, A.I.A. and H.P.S.; writing—original draft preparation, A.I.A. and H.P.S.; writing—review and editing, A.Z.A.; visualization, A.I.A.; supervision, A.Z.A.; project administration, A.Z.A.; funding acquisition, A.Z.A. All authors have read and agreed to the published version of the manuscript.

Funding: This study was financed by the European Union—NextGenerationEU—through the National Recovery and Resilience Plan of the Republic of Bulgaria, project NO. BG-RRP-2.013-0001.

Data Availability Statement: The data presented in this study are available on request from the corresponding author.

Acknowledgments: The authors are very grateful to the anonymous reviewers whose valuable comments and suggestions improved the quality of the paper.

Conflicts of Interest: The authors declare no conflicts of interest.

Abbreviations

The following abbreviations are used in this manuscript:

NDVI	Normalized difference vegetation index
SAVI	Soil adjusted vegetation index
EVI2	Enhanced vegetation index 2
NIRI	Near infra-red index
CNN	Convolutional neural networks
LSTM	Long short-term memory
MLP	Multi-layer perceptron

References

1. Food and Agriculture Organization of the United Nations (FAO). Statistical Databases. 2018. Available online: https://faostat.fao.org/ (accessed on 12 September 2025).
2. Padhiary, M.; Rani, N.; Saha, D.; Barbhuiya, J.A.; Sethi, L.N. Efficient precision agriculture with Python-based Raspberry Pi image processing for real-time plant target identification. *Int. J. Res. Anal. Rev.* **2023**, *10*, 539–545.
3. Raghu Vamsi, P.; Upadhyay, P.K. Prediction Model for Precision Agriculture Using Machine Learning. In *Data Science and Communication*; Tavares, J.M.R.S., Rodrigues, J.J.P.C., Misra, D., Bhattacherjee, D., Eds.; Springer: Singapore, 2024; pp. 1–15. [CrossRef]
4. Abdullahi, H.S.; Sheriff, R.E. Introduction to deep learning in precision agriculture: Farm image feature detection using unmanned aerial vehicles through classification and optimization process of machine learning with convolution neural network. In *Cognitive Data Science in Sustainable Computing, Deep Learning for Sustainable Agriculture*; Poonia, R.C., Singh, V., Nayak, S.R., Eds.; Academic Press: Cambridge, MA, USA, 2022; pp. 81–107. [CrossRef]
5. Zahra, S.; Ruiz, H.; Jung, J.; Adams, T. UAV-Based Phenotyping: A Non-Destructive Approach to Studying Wheat Growth Patterns for Crop Improvement and Breeding Programs. *Remote Sens.* **2024**, *16*, 3710. [CrossRef]

6. Mia, P.; Mamun, M.A. Precision Agriculture Using Machine Learning. 2025. Available online: http://ar.cou.ac.bd:8080/handle/123456789/124 (accessed on 10 August 2025).
7. Khan, A.; Patil, C.H.; Vibhute, A.D.; Mali, S. Application of image processing and machine learning techniques for vegetation cover classification in precision agriculture. In *Image Processing with Python*; IOP Publishing: Bristol, UK, 2024; pp. 11-1–11-29. [CrossRef]
8. Deng, L.; Mao, Z.; Li, X.; Hu, Z.; Duan, F.; Yan, Y. UAV-based multispectral remote sensing for precision agriculture: A comparison between different cameras. *ISPRS J. Photogramm. Remote Sens.* **2018**, *146*, 124–136. [CrossRef]
9. Ganeva, D.; Roumenina, E.; Dimitrov, P.; Gikov, A.; Jelev, G.; Dyulgenova, B.; Valcheva, D.; Bozhanova, V. Remotely Sensed Phenotypic Traits for Heritability Estimates and Grain Yield Prediction of Barley Using Multispectral Imaging from UAVs. *Sensors* **2023**, *23*, 5008. [CrossRef]
10. Atanasov, A. Possibilities of small robotic UAVs for surveillance of agricultural areas in Southern Dobruja. *Bulg. J. Crop Sci.* **2024**, *61*, 100–108. [CrossRef]
11. Chlingaryan, A.; Sukkarieh, S.; Whelan, B. Machine learning approaches for crop yield prediction and nitrogen status estimation in precision agriculture: A review. *Comput. Electron. Agric.* **2018**, *151*, 61–69. [CrossRef]
12. Omia, E. Remote sensing in field crop monitoring: A comprehensive review of sensor systems, data analyses and recent advances. *Remote Sens.* **2023**, *15*, 354. [CrossRef]
13. Andujar, D.; Martinez-Guanter, J. An overview of precision weed mapping and management based on remote sensing. *Remote Sens.* **2022**, *14*, 3621. [CrossRef]
14. Forkuor, G.; Hounkpatin, O.K.L.; Welp, G.; Thiel, M. High-resolution mapping of soil properties using remote sensing variables in south-western Burkina Faso: A comparison of machine learning and multiple linear regression models. *PLoS ONE* **2017**, *12*, e0170478. [CrossRef]
15. Sheffield, J. Satellite remote sensing for water resources management: Potential for supporting sustainable development in data-poor regions. *Water Resour. Res.* **2018**, *54*, 9724–9758. [CrossRef]
16. Yang, C. Remote sensing and precision agriculture technologies for crop disease detection and management with a practical application example. *Eng. J.* **2020**, *6*, 528–532. [CrossRef]
17. Hopoocolor. Available online: https://www.hopoocolor.com/product/detail/HPCS320.html (accessed on 10 August 2025).
18. Elimex. Available online: https://elimex.bg/product/67884-ured-anemometar-termometar-hidrometar-va8021 (accessed on 10 August 2025).
19. Rouse, J.W.; Haas, R.H.; Schell, J.A.; Deering, D.W.; Harlan, J.C. *Monitoring the Vernal Advancement and Retrogradation of Natural Vegetation*; NASA/GSFC: Greenbelt, MD, USA, 1974; p. 371.
20. Huete, A.R. A soil-adjusted vegetation index (SAVI). *Remote Sens. Environ.* **1988**, *25*, 295–309. [CrossRef]
21. Jiang, Z.Y.; Huete, A.R.; Didan, K.; Miura, T. Development of a two-band enhanced vegetation index without a blue band. *Remote Sens. Environ.* **2008**, *112*, 3833–3845. [CrossRef]
22. Stevens, F.R. *Bridging the Landsat Data Gap: Evaluating ASTER as an Alternative*; University of Florida: Gainesville, FL, USA, 2009.
23. Atanasov, A. A drone-based study on the possibilities of agricultural crop assessment using reflectance index in NIR. *Bulg. J. Agric. Sci.* **2024**, *30*, 1136–1140.
24. Mapir. Available online: https://www.mapir.camera/en-gb/collections/survey3/products/survey3w-camera-red-green-nir-rgn-ndvi (accessed on 10 August 2025).
25. DJI. Available online: https://www.dji.com/support/product/phantom-4-adv (accessed on 10 January 2026).
26. Pix4D. Available online: https://www.pix4d.com/download-software/ (accessed on 10 August 2025).
27. IBM. Available online: https://www.ibm.com/products/spss-statistics (accessed on 10 August 2025).
28. Farooq, M.; Wahid, A.; Kobayashi, N.; Fujita, D.; Basra, S.M.A. Plant drought stress: Effects, mechanisms and management. *Agron. Sustain. Dev.* **2009**, *29*, 185–212. [CrossRef]
29. Liu, Y.; Wang, S.; Chen, J.; Chen, B. Rice yield prediction and model interpretation based on satellite and climatic indicators using a transformer method. *Remote Sens.* **2022**, *14*, 5045. [CrossRef]
30. Sun, J.; Di, L.; Sun, Z.; Shen, Y.; Lai, Z. County-level soybean yield prediction using deep CNN-LSTM. *Sensors* **2019**, *19*, 4363. [CrossRef] [PubMed]
31. Zhou, W.; Song, C.; Liu, C.; Fu, Q.; An, T.; Wang, Y.; Sun, X.; Wen, N.; Tang, H.; Wang, Q. A prediction model of maize field yield based on the fusion of multitemporal and multimodal UAV data: A case study in Northeast China. *Remote Sens.* **2023**, *15*, 3483. [CrossRef]
32. Qiao, D.; Yang, J.; Bai, B.; Li, G.; Wang, J.; Li, Z.; Liu, J.; Liu, J. Non-Destructive Monitoring of Peanut Leaf Area Index by Combing UAV Spectral and Textural Characteristics. *Remote Sens.* **2024**, *16*, 2182. [CrossRef]
33. Fu, H.; Li, J.; Lu, J.; Lin, X.; Kang, J.; Zou, W.; Ning, X.; Sun, Y. Prediction of soybean yield at the county scale based on multi-source remote-sensing data and deep learning models. *Agriculture* **2025**, *15*, 1337. [CrossRef]

34. Aslam, A.; Farhan, S. Enhancing rice yield prediction: A deep fusion model ResNet50-LSTM with multi-source data. *PeerJ Comput. Sci.* **2024**, *10*, e2219. [CrossRef] [PubMed]
35. Khallikkunaisa, S.D.J.; Teja, V.T.; Raj, E.S.; Tharun, R. Comprehensive analysis of crop yield prediction using deep learning and remote sensing techniques. *Preprints* **2025**. [CrossRef]

Disclaimer/Publisher's Note: The statements, opinions and data contained in all publications are solely those of the individual author(s) and contributor(s) and not of MDPI and/or the editor(s). MDPI and/or the editor(s) disclaim responsibility for any injury to people or property resulting from any ideas, methods, instructions or products referred to in the content.